PNAS
www.pnas.org

Supplementary Information for

The Emergence of a Functionally Flexible Brain During Early Infancy

Weiyan Yin, Tengfei Li, Sheng-Che Hung, Han Zhang, Li Wang, Dinggang Shen, Hongtu Zhu, Peter J. Mucha, Jessica R. Cohen, Weili Lin

Corresponding author: Weili Lin, PhD

Email: Weili_lin@med.unc.edu

This PDF file includes:

Table of Contents

SI-1: The potential origins of neural flexibility

While we could speculate the potential origins of the MR measured neural flexibility, it is unlikely that we will be able to provide conclusive evidence demonstrating the origins of neural flexibility measured by resting fMRI. Perhaps animal studies using multi-channel microelectrode array recordings could provide insights into the origins of MR-measured flexibility. However, this is clearly beyond the scope of our manuscript. Nevertheless, we will attempt to address this question from three different aspects: i) the potential origins of BOLD effects; ii) the ability to capture cognitive statuses using the sliding window approaches; and iii) recently published results on neural flexibility.

i) The potential origins of BOLD: Functional MR has become the method of choice to reveal brain functional networks. Numerous studies and evidence have largely supported that spontaneous fluctuations of BOLD signal reflect ongoing neuronal processes (1, 2). A recent publication by Lu et al. (1), however, argued that the widely held "neurocentric" model may not account for all variances observed in BOLD signal fluctuations and concluded that BOLD signal fluctuations may have more complex cellular origins. Nevertheless, their results remain to support that BOLD signal fluctuations reflect underlying neuronal activity. Together, it is reasonable to conclude the purported neural origin of flexibility using resting functional MRI.

ii) The ability to capture cognitive statuses using sliding window approaches: Using the sliding window approach as in our study, recent studies have demonstrated that the human brain is a dynamic system, with changing cognitive states and functional connectivity even during a short scan session (3-6). These results suggested the presence of different types of mental activities during a resting period (4, 7), and the predominance of activity can affect the functional connectivity and modular organization (8). Conversely, recent studies have also argued that the sliding window approach could generate spurious findings that were largely attributed by a short window length and/or motion artifacts. To this end, using simulation and human studies, it has been suggested that a window length of 40s-100s could minimize spurious dynamics (6, 9-13). Therefore, our choice of a window length of 60s is highly consistent with the range of the suggested window lengths. Furthermore, we demonstrated that the conclusions of our studies are not altered using two other window lengths (i.e. 40s, 80s) as shown in Fig. S10 and SI-10.

Regarding motion artifacts, two main approaches were employed in our study to minimize effects of motion, including pre-processing steps and the use of wavelet-denoising pipeline (14, 15). As a result, subjects with severe motion artifacts were excluded in our analysis (please see Methods). Thus, though spurious effects might influence the results, our approaches have minimized these potential factors.

iii) Recently published results: Finally, the concept of brain flexibility has recently been proposed by Bassett et al. (16) utilizing a multilayer network in task-fMRI studies. In their studies, brain flexibility is associated with learning new motor skills. Specifically, brain flexibility increases and then decreases during learning a new motor skill. More importantly, brain flexibility in one learning session predicts the amount of learning in a future session. In a following study by the same group (17), they also provided evidences that the brain flexibility oscillated across task executions, and higher frontal flexibility is cognitively beneficial for working-memory performance. Additionally, brain flexibility could also serve as a biomarker for identifying subjects with genetic risks of developing schizophrenia (18). Finally, recent resting-state study with HCP data also indicated brain flexibility could predict task performance (19). These previous studies shed light on the importance of brain flexibility associating with learning and executive functions.

In summary, although it is beyond the scope of our study to provide experimental evidence regarding the origins of neural flexibility, it is highly plausible that neural flexibility provides quantitative measures of temporal stability of a brain region in association with a specific functional module, which could offer biologically meaningful insights into how a brain regions may contribute to different cognition responding to different mental demands at a given time. In the context of our study, brain flexibility may provide an invaluable tool to characterize brain functional development. In particular, as implicated by Bassett et al, changes of flexibility are associated with learning a new motor skill. Considering interaction/learning with external environmental stimuli plays a key role in the maturation and specialization of brain functions during early infancy, the assessments of neural flexibility may provide biologically meaningful neurodevelopmental characteristics during early infancy.

SI-2: Across age group comparisons

To evaluate brain regional developmental patterns, we compared regional neural flexibility between every pair of adjacent age groups using a two-sample t-test (Fig. S1), $p<0.05$, uncorrected. The anatomical locations of these regions are summarized based on their lobar distribution (Fig. S1b), which reveals four different patterns at different ages. A marked change of neural flexibility is observed during the first three months of life with the largest number of brain regions demonstrating significant changes in flexibility. Importantly, a larger number of regions show a reduction (19 vs. 13) in neural flexibility during this time period and many of them are in the parietal and occipital lobes. Between months 3 – 12, a larger number of brain regions exhibit a significant increase than decrease in neural flexibility. Conversely, most of the regions show a reduction in neural flexibility between 12 – 18 months, followed by an increased neural flexibility for all regions between 18 – 24 months. Finally, the majority of brain regions in the frontal lobe

display an increase of neural flexibility during the first two years of life, which may reflect the effects of external stimuli shaping the continuing maturation processes in the frontal lobe.

SI-3: Brain atlas and network selection

While adult brain functional atlases are available (20-23), a widely accepted infant brain functional atlas is largely lacking. Although there are a few published papers reporting infant atlas/networks (24-27), the validity and consistency of these results at different ages are yet to be determined. To a large extent, this lack of a widely accepted infant brain functional atlas is not surprising since it is almost impossible to conduct task-based functional MRI in infants with the exception of basic brain functions (28-38). Thus, adopting adult brain atlases and warping them to infant brains has been widely used in current pediatric studies (39-41). In this study, we adopted this approach to provide insights into the developmental trajectories of neural flexibility in different brain functional networks during early infancy based on the Shen268 atlas (20).

Since an atlas was warped to the infant brains, ROI parcel homogeneity may vary across subjects and ages. To further determine if our results could be affected by ROI parcel homogeneity, we adopted the definition of parcel homogeneity proposed by Gordon et al. (42) and calculated the parcel homogeneity of each ROI for each subject at different ages. For each ROI, we computed voxel-wise whole brain connectivity patterns for all voxels within a given ROI. We then used principal component analysis to determine the percent of total variances of all connectivity patterns that can be explained by the largest principal component. As discussed by Gordon et al. (42), smaller parcels would be intrinsically more homogeneous. In our study, brain atlas was deformed back to the subject space, yielding different ROI sizes for the same ROI at different subjects/ages. In order to minimize the effect of the ROI size, we regressed the effect of ROI size from raw homogeneity and used residuals to generate homogeneity trajectories for each ROI. Fig. S2a shows the typical homogeneity trajectory for a given brain region, demonstrating no clear age effects during the first two years of life. The blue line is the best fit for the homogeneity trajectory from birth to 2 years of age. Besides, we found no age effects for the measured homogeneity across all the regions (Fig. S2b, LME model, F-test, $p > 0.05$, FDR corrected), suggesting that regional homogeneity is consistent across all ages.

Nine resting-state functional networks were included in this study, including the medial frontal network, frontoparietal network, default network, subcortical network, motor network, visual I network, visual II network, visual association network, and cerebellum network. These networks were initially defined using the Shen268 atlas (20). However, owing to the observed low flexibility pattern in the cerebellum/brainstem regions, as well as findings from the Smith networks (43), we excluded

cerebellum/brainstem regions from the predefined networks of the Shen268 atlas and created a cerebellum network. Additional networks, including the salience network, dorsal attention network, ventral attention network, working memory network, and inhibition network were defined based on references (44-48). The anatomical locations of each network are summarized in Fig. S3.

While the definitions of these functional networks in our study may not be standard for infants, we believe that the brain regions comprising the basic functional networks should be appropriate. In particular, a large body of evidence has consistently demonstrated that the topology and behaviors of basic brain functions mature rapidly during the first year of life (49-54). In contrast, the definitions of higher-order functional networks may be questionable since integration of these higher order networks may not be completed during early infancy. Nevertheless, some published reports have demonstrated the presence of higher order brain functional networks in infants. Doria et al. (55) studied 70 preterm infants (born between 29 and 43 weeks of postmenstrual age) using resting functional MRI. A wide array of brain functional networks using similar definitions as those in our manuscript was characterized using both ICA as well as seed-based approaches. They reported that most of the brain functional networks reported in adults are also recognizable in preterm infants, although they are mostly fragmented at 30wks of postmenstrual age. By term, most of the networks are integrated. Gao et al. (56) focused on the development of the default mode network in typically developing children 0-2 years of age. Similarly, they reported that a primitive and incomplete default mode network is presence at birth. By 2 years old, an adult-like default mode network is present. Since these results were obtained at a resting state, one could argue that the presence of adult-like resting functional networks during early infancy may not represent that the brain functions associated with these networks are already online during early infancy. Dehaene-Lambert et al. (57) used task based functional MR in awake infants to evaluate how infants (3 months old) reacted to their native language. Specifically, they reported that left lateralized frontal regions similar to adults exhibited activation to normal but not reversed speech. Additional activation in the right prefrontal cortex was observed as well. They thus concluded, “precursors of adult cortical language areas are already active in infants, well before the onset of speech production.” Similarly, Grossmann et al. (58) used NIRS to study the development of voice processing in infants from birth to 1yr old. They reported that a greater response was observed in bilateral superior temporal cortex with human voice than that of non-vocal sound, and voice sensitive brain functions emerged between 4 and 7 months of age. Additional studies using NIRS suggest the presence of higher order brain functions including but not limited to recognizing mother’s faces in infants (59), auditory perception (60), motor and oculomotor planning (61), and processing social information (62). In summary, while there is not a widely accepted infant brain functional atlas and the use of adult functional atlases for infant applications may not be optimal, numerous reported results appear to provide some evidence in support of the use of adult brain function network definitions in the absence of a better solution.

Finally, to further demonstrate the robustness of our results, AAL (63) and CC200 (21) atlases were further applied. The numbers of ROI are 90 and 200 for the AAL and CC200 atlases, respectively. Therefore, in addition to evaluate the robustness of our results regarding the choice of atlases, the use of three different atlases also enables us to evaluate effects of different ROI numbers - 90, 200, and 268. The spatiotemporal distribution of brain neural flexibility was shown in Fig. S4a-S4b. The overall patterns of neural flexibility remain consistent with those using the Shen268 atlas as reported in the main body of the paper. (Fig. S4c-S4d). In addition, we quantitatively compared the voxel-wise distributions of neural flexibility between Shen268 vs AAL as well as Shen268 vs CC200, respectively (Fig. S4e). Specifically, we labeled each voxel with the neural flexibility value of its ROI assignment, and then calculated the spatial similarity (i.e. Pearson's correlation coefficient) of the overlapped voxels between atlases. Our results indicated the spatial distributions of neural flexibility using AAL and CC200 are significantly correlated with that using the Shen268 atlas (Pearson's correlation t-test, $p < 10^{-16}$, FDR corrected).

SI-4: Definition of the flexible club

In the main text, we defined brain flexible club as the regions with neural flexibility that are significantly higher than the whole brain averaged flexibility. Specifically, we proposed a statistical method to evaluate whether brain regional flexibility is significantly different than that of the whole brain averaged flexibility. For each subject, we calculated the whole brain averaged flexibility. For each region at a given age group, we performed group comparisons of regional flexibility and whole brain averaged flexibility using a paired t-test. Brain regions were then separated into three groups based on the statistical results ($p < 0.05$, uncorrected) (Fig. S5a): (1) regions with significantly higher flexibility than that of the whole brain (red), (2) regions with similar flexibility to that of the whole brain (orange), (3) regions with significantly lower flexibility than that of the whole brain (blue). The number of regions exhibit significantly higher/lower flexibility than that of the whole brain is summarized in the Table S1. The brain regions with significantly higher/lower neural flexibility than that of the whole brain were shown in Fig. 4 and Fig. S5b, respectively.

SI-5: Model selection for fitting longitudinal developmental trajectories

To evaluate the developmental trajectories of neural flexibility, we compared the results using a linear mixed-effects model (LME) and a Generalized Addictive Mixed Model (GAMM), separately. A Linear Mixed-Effects model was fit to the data with a random intercept for each subject. A Generalized Addictive Mixed Model was also used to delineate the longitudinally developmental trajectory of brain dynamic features. The model included age as a covariate and subject ID as the random intercept:

$$Y_i(t) = f(t) + \alpha_i + e_i(t)$$

where $Y_i(t)$ is the brain feature for the i^{th} subject at time t, α_i is the i^{th} random intercept effect and $e_i(t)$ is the random noise. Specifically, α_i $(i = 1,2, \dots, n)$ are independent and identically distributed (i.i.d), with a normal distribution $N(0, \sigma_\alpha^2)$, and $e_i(t)(i = 1,2, \dots, n, t < T)$ are i.i.d. normally distributed with $N(0, \sigma_e^2)$. Here, $f(t)$, σ_α, σ_e are unknown parameters. With the observations of brain features at different ages, we obtained an estimate $\hat{f}(t)$ of $f(t)$ by fitting the nonparametric parameters with cubic spline, where smoothing parameters were chosen to minimize the Generalized Cross Validation (GCV) errors (64). Standard deviation and 95% confidence intervals of the fixed effect were calculated through the Bayesian posterior covariance matrix (65). The model curve fitting plots used the R package mgcv and itsadug (66).

By comparing the trajectories and GCV errors between the GAMM and LME models in network fitting (Table S2), though the AIC value of GAMM was always lower than that of LME, the developmental neural flexibility trajectories of the whole brain, medial frontal network, default network, subcortical network, motor network, visual II network, visual association network, cerebellum network, ventral attention network, inhibition network are almost identical to the LME fitting (Fig. S6a). The GCV difference is less than 2%, suggesting that the LME and GAMM models perform similarly for fitting these trajectories. However, the GCV differences are relatively larger in the frontoparietal network, visual I network, salience network, dorsal attention network, and working memory network. Though the trajectories of GAMM model show slight differences when compared to that obtained using the LME model in these parameters, the GCV difference is still low (i.e. less than 5%) and the LME model could still represent the general developmental patterns. Finally, since the LME model provides quantitative measure of the slopes to represent the developmental paces but not the GAMM model, we have chosen the LME model in our network-level analysis.

Additionally, the GCV differences in ROI fitting models also exhibit similar pattern, with 256/268 regions showing GCV difference less than 5% (Fig. S6c), suggesting LME could represent the general developmental patterns for ROI-level analysis.

SI-6: Quantifying brain functional maturation using rsfMRI: neural flexibility vs connectivity strength

RsfMRI has been utilized to characterize early brain functional development (50, 67, 68). Specifically, the mean connectivity strength within selected brain functional networks are commonly employed to quantify the maturation of these functional networks. To compare the potential differences between neural flexibility and connectivity strengths for characterizing brain functional development during early infancy,

the connectivity strengths of nine commonly reported adult functional networks and five cognitive flexibility associated networks were calculated and the developmental trajectories are shown in Fig. S7 (red lines). Bassett et al. (16) observed that changes in neural flexibility were associated with learning a new motor skill. For early brain development, learning via external environmental stimuli plays a vital role in brain functional maturation and specialization. Therefore, we proposed that the measure of neural flexibility could provide a more direct assessment of brain functional maturation than that of connectivity strength. Indeed, infants' gross and fine motor abilities develop gradually during the first two years of life, as babies start to roll over, sit, stand, crawl and walk gradually. Our finding of increased neural flexibility in motor associated regions may more accurately reflect the maturation of motor skills when compared to that reported using functional connectivity strengths, which show an age related reduction (67). Along the same vein, the neural flexibility trajectories of higher-order brain functional networks also show continuing increases over the first two years of life. In contrast, the connectivity strengths of the higher-order functional networks are observed with a stable/decreased pattern during the first two years of life. While it was previously suggested that higher-order brain functions do not emerge until school age or beyond, more recent evidence has suggested the presence of rudimentary higher-order brain functions, including processing linguistic information (57, 69), attention (70), memory processing (71, 72), processing social interaction (73) and executive functions (74). Therefore, our results appear to be consistent with these recent findings, with a continuing increase of brain neural flexibility during the first two years of life.

Finally, the primary visual network exhibits a temporally stable degree of neural flexibility, while visual II and visual association networks show a slow but increasing neural flexibility during the first two years of life. In contrast, visual I, visual II and visual association networks all exhibit a rapid increase in connectivity strength, especially in the first 6 months of age. One could argue that the increased connectivity strengths during the first 6 months of life represent active visual maturation. While it has been well documented that visual function matures earlier than other brain functions during infancy with the primary visual function maturing first, followed by VII and visual association functions. The measures of neural flexibility appear to be more consistent with these previously reported results with a stable trajectory for visual I while visual II and visual association exhibit slightly increased neural flexibility with age.

In summary, our results demonstrate that the trajectories of brain neural flexibility at both the network and regional levels may be indicative of brain functional maturation during early brain development. Functional networks implicated to mature early show a relatively low change in flexibility over the first two years of life. In contrast, less mature and/or emerging functional networks exhibit continuing increase in flexibility during this time period.

SI-7: The relations between brain neural flexibility and behavioral outcomes

The correlation between neural flexibility and GCA scores was evaluated at brain regional and network level, respectively. Brain networks and regions with a significant correlation (Pearson's correlation T-test, $p < 0.05$, uncorrected) were shown in Fig. S8. Visual regions were found to be negatively correlated with GCA in most of the age groups. In contrast, some regions associated with cognitive flexibility were positively associated with GCA scores, including the inferior temporal gyrus at month 12, part of superior temporal gyrus at month 18, and the temporoparietal junction at month 24. However, due to the limited sample sizes, only one region in the calcarine at birth did pass the false discovery rate correction.

SI-8: Adolescent and adult datasets

Eight-seven and seventy-six subjects from the Adolescent Brain Cognitive Development Dataset (75) (ABCD) and the Human Connectome Project (76) (HCP), respectively, were included in this manuscript to compare results obtained from pediatric subjects.

ABCD subjects were scanned using 3T MR scanners (Siemens Prisma). T1/T2-weighted images, as well as resting-state fMRI images were acquired. Resting-state fMRI images were acquired with eyes open and passive viewing of a cross hair. T1-weighted images were acquired with a voxel size of $1 \times 1 \times 1\ mm^3$ (Repetition time =2500 ms, echo time =2.88 ms). T2-weighted images were acquired with a voxel size of $1 \times 1 \times 1\ mm^3$ (Repetition time =3200 ms, echo time =565 ms). fMRI images were acquired with a voxel size of $2.4 \times 2.4 \times 2.4\ mm^3$ (repetition time=800 ms, echo time=30 ms, 383 volumes).

HCP subjects were scanned using 3T MR scanners (Siemens Skyra). T1/T2-weighted structural images and resting-state fMRI images (eyes open and fixation on a crosshair) were used to perform analysis. T1-weighted images were acquired with a voxel size of $0.7 \times 0.7 \times 0.7\ mm^3$ (Repetition time =2400 ms, echo time =2.14 ms). T2-weighted images were acquired with a voxel size of $0.7 \times 0.7 \times 0.7\ mm^3$ (Repetition time =3200 ms, echo time =565 ms). fMRI images were acquired with a voxel size of $2 \times 2 \times 2\ mm^3$ (repetition time=720 ms, echo time=33.1 ms, 1200 volumes).

An identical preprocessing pipeline was applied to both ABCD and HCP datasets. The sliding window widths were set as 75 volumes for ABCD and 83 volumes for HCP, to keep the window duration time close to 60 seconds, similar to our study. The step size was set as 1 volume.

SI-9: Effects of the resolution and interlayer coupling parameters

The proper use of any community detection method necessarily encounters questions about the resolution scale at which communities are identified and whether meaningful communities at other scales are not detected (16, 77). By considering multiple values of the resolution parameter, we may reveal different scales of community numbers (78, 79), i.e. smaller gamma typically results in larger modules whereas larger gamma yields smaller modules. In the multilayer situation, different strengths of the inter-layer coupling parameter also influences the detected dynamic structures (80). In order to test the stability of neural flexibility patterns across different choices of resolution and interlayer coupling parameters, we considered resolution (gamma) parameters from 0.2 to 2 and coupling (omega) parameters from 0.2 to 2.

The absolute values of neural flexibility depend on the choice of gamma and omega. However, similar developmental patterns were obtained with a wide range of parameters (gamma from 0.6 to 2, omega from 0.2 to 2) (Fig. S9). In addition, we compared the spatial similarity of the distribution of brain neural flexibility, by calculating the Pearson's correlation of neural flexibility across ROIs as calculated with different gamma and omega pairs. A high spatial similarity ($r > 0.9$) of the distribution of neural flexibility within each age group was revealed, indicating a highly stable spatial distribution pattern of neural flexibility across different community detection parameters.

SI-10: Effects of the window length

To construct multilayer networks using a sliding window approach, it is necessary to choose a window length. If the window length is too long, the ability to estimate neural flexibility will be compromised. Conversely, if the window length is too short, the statistical power for estimating functional connectivity will be reduced. In the main text, we reported the results using a window length of 60 seconds, which is well within the range of window lengths (i.e. 40s – 100s) suggested in several previously published studies (9-13). Nevertheless, it is essential to determine if our conclusions would be altered should a different window length is used. To this end, we conducted additional data analyses using two different window lengths, 40s and 80s, respectively. The new results are provided in the Fig. S10. Even though the absolute values of neural flexibility are changed using different window lengths, the developmental patterns of neural flexibility remain similar to those using a window length of 60 seconds. Furthermore, we compared the spatial similarity of the distribution of brain neural flexibility, by calculating the Pearson's correlation of neural flexibility across ROIs as calculated with different window lengths. A spatial similarity over 0.9 was obtained using these different window lengths, indicating that the spatial patterns of neural flexibility are highly similar.

SI-11: Multilayer network model: positive-only and signed models

We adopted the quality function Q as proposed by Mucha et al. (80) in our study, which has been used in several neuroscience studies to evaluate multilayer networks (16-18, 81, 82). The quality function is:

$$Q = \frac{1}{2\mu}\sum_{ijsr}\left[\left(A_{ijs} - \gamma_s\frac{k_{is}k_{js}}{2m_s}\right)\delta_{sr} + \delta_{ij}\omega_{jsr}\right]\delta(g_{is}, g_{jr})$$

where the adjacency matrix of layer s has components A_{ijs}. Note the layer here refers to an adjacency matrix of a given sliding window. The resolution parameter of layer s is γ_s; g_{is} and g_{jr} are the community assignments of node i in layer s and node j in layer r, respectively; ω_{jsr} is the inter-layer coupling strength parameter connecting node j in layers r and s; μ is the total edge weight in the network, calculated as $\mu = \frac{1}{2}\sum_{jr}\kappa_{jr}$; $k_{js} = \sum_i A_{ijs}$ is the intra-layer strength of node j in layer s; the inter-layer strength of node j in layer s is $c_{js} = \sum_r \omega_{jsr}$; the strength of node j in layer s is $\kappa_{js} = k_{js} + c_{js}$; and m_s is the total edge weight in layer s, defined as $m_s = \frac{1}{2}\sum_{ij} A_{ijs}$. We kept resolution parameters constant across layers ($\gamma = \gamma_s$) and the same weight ω for all inter-layer connections that were present.

This model limits the components A_{ijs} to be positive only. Thus, in our study, we adopted a widely used approach by taking the absolute values of the connectivity strengths (83-88). In so doing, our results consider all connections equally independent of the signs. In order to remove weak and random connections, a p-value for each correlation coefficient was estimated using the MATLAB function corrcoef and only connections significantly different from zero were retained (Pearson's correlation T-test, $p < 0.05$, FDR corrected). To further test the robustness of our results, we had re-evaluated brain neural flexibility by only using positive values, an approach that has also been employed in the several previously published studies (41, 77, 89). The same resolution and coupling parameters as those using the absolute values of connectivity were used. Although the values of the estimated neural flexibility were reduced when only positive connections were used when compared to the use of absolute connectivity (Fig. S11), the results showed consistent developmental trajectories as those reported in our manuscript. Furthermore, high spatial similarity was obtained ($r > 0.77$), suggesting a high spatial similarity of brain neural flexibility between using absolute and positive values.

In contrast, the biological meanings of negative correlations remains elusive (90). In particular, it has been argued that the required pre-processing steps of resting functional MR may have led to the presence of negative correlations. Nevertheless, to the best of our knowledge, a consensus regarding the biological meaning of negative correlations remains lacking (91, 92). Nevertheless, we have evaluated the potential impacts on the results if the signs of the connection are considered. To further evaluate the effects of the negative correlations, we modified the quality function appropriately as:

$$Q_{\pm} = \frac{1}{2\mu^{+} + 2\mu^{-}} \sum_{ijsr} \left[\left(A_{ijs} - \left(\gamma_s^{+} \frac{k_{is}^{+} k_{js}^{+}}{2m_s^{+}} - \gamma_s^{-} \frac{k_{is}^{-} k_{js}^{-}}{2m_s^{-}} \right) \right) \delta_{sr} + \delta_{ij} \omega_{jsr} \right] \delta(g_{is}, g_{jr})$$

where the definitions of these parameters are the same as the above, with positive and negative signs to indicate the positive and negative elements of A_{ijs}, respectively. In contrast to the quality equation in which signs of connectivity are not considered, three parameters need to be determined: two resolution parameters and one coupling parameter. For consistency, we set these parameters to unity. The resulting developmental trajectories when signs were considered are mostly consistent with the results using absolute values of connectivity (Fig. S11). Nevertheless, the spatial similarity was reduced, suggesting some discrepancies in results with and without considering signs of the connectivity. Although several factors may potentially contribute to these observed differences, the differences of the multilayer modularity model and the additional resolution parameter (γ_s^{-}) specifically for the negative values are highly plausibly contributing to the observed differences. Specifically, γ_s^{-} was set to be identical to γ_s^{+} which may not be necessarily valid (93). More evaluation will be needed to determine the choices of γ_s^{-} and γ_s^{+}, which is beyond the scope of our study.

SI-12: Limitations

There are several limitations in our study. First, changes of brain tissue properties during early infancy may lead to MR signal changes. Specifically, the dehydration processes of the human brain tissue after birth leads to T1 and T2 changes (94), which in turn will affect tissue contrast in T1-weighted (T1w) and T2-weighted (T2w) images. One of the most widely recognized examples is the contrast reversal between gray and white matter in T1w images during the first year of life; the white matter exhibits a lower signal up to 6-9 months old and the signal becomes higher after 9 months old than that of gray matter. This temporal reversal of gray/white contrast could affect our ability to accurately co-register resting functional MR images since T1w images were used for registration across subjects and ages. Our team has developed novel image analysis approaches mitigating the effects of contrast reversal in T1w images during infancy, minimizing confounding factors resulting from inaccurate registration (95).

In the context of fMRI, changes of T2* could potentially affect the sensitivity of BOLD contrast. It has been reported that the infant brain has a longer T2* when compared to adults (96-98), suggesting that a longer TE can be used for the gradient echo EPI sequence. However, the infant brain T2* continues to decrease with age and becomes similar to that of adult brains around 9 months of age (97). Furthermore, reported increased T2* in the infant brain is not spatially homogeneous but rather anatomical location dependent. Therefore, although it is possible to potentially adjust TE of the EPI sequence for infants younger than 9 months old, an optimal TE for the entire brain is unlikely. In addition, T2* also depends on the spatial resolution of images with a larger voxel leading to a shorter T2* when compared to measured

using a smaller voxel. Finally, adjusting TE based on the age of the infants could lead to additional biases. Therefore, we have used a fixed TE for our study. It is possible that sensitivity of detecting BOLD signal may be lower for infants younger than 9 months of age. However, it should not affect the overall conclusions of our results as evident from the trajectories of the measured neural flexibility.

Second, the number of scanning volumes (i.e. 150 volumes, 5 minutes) is less than that proposed by the Human Connectome Protocol (76, 99). While a longer acquisition time and a larger volume of rsfMRI are clearly desirable, since all of the subjects were imaged during natural sleep without sedation, the choice of imaging volumes (duration) reflected a compromise on the duration of resting functional MR in order to maximize the success rate of obtaining usable resting fMRI in imaging typically developing children without sedation.

Finally, information on sleep stages during the acquisition of resting fMRI was not available. This limitation is not unique to our study. In fact, all of the functional MRI datasets focusing on early brain development do not have sleep information owing to several practical difficulties of imaging non-sedated typically developing children. In particular, MR is highly sensitive to motion artifacts. Fitting addition EEG caps on infants/toddlers could make it difficult for the participants to fall asleep and will be more likely to wake-up and move during MR imaging sessions, leading to decreased success rates of obtaining usable MR images. In addition, although MR compatible EEG is available, it has not been widely used to technical difficulties. Therefore, the approaches employed in our study although not optimal are the best that one could do without a high failure rate for acquiring usable images.

Some results from adult studies, however, could provide some insights into how sleep could affect brain functional connectivity. Although results differ among some reported results, including the extent of BOLD signal fluctuation, connection strengths, and spatial extent, between wakefulness and sleep, similar brain functional networks are consistently observed independent of consciousness status. Horovitz et al. (100) conducted a study aiming to determine how varying levels of consciousness, including resting wakefulness and light sleep, affect resting functional connectivity. Concurrently acquired EEG was employed to determine the depth of sleep. An increased BOLD fluctuation was observed in multiple brain regions, including the visual cortex and regions in default mode network during sleep when compared to wakefulness. The increased fluctuation in the visual cortex correlates with the depth of sleep. In contrast, spatial topologies of the visual cortex and DMN are comparable between wakefulness and sleep. A different study by Horovitz et al. (101) further reported a reduced involvement of brain regions in the frontal lobe of the default mode network during natural sleep. However, these results compared a wakefulness state and sleep. Since all of our subjects were at sleep, the potential differences of functional connectivity arising from different stages of sleep need to be discussed. It is reasonable to assume that different subjects were at different stages of sleep during the acquisition of

resting functional MR. As a result, the effects of different sleep stages from subjects to subjects could be averaged out for group comparisons. Furthermore, the sleep pattern of infants change around 3-4 months of age, from two stages (i.e. quite stage, active stage) to adult-like (102). In this case, if different stages of sleep during acquisition could impact on our results, we should expect to find some discontinuities around this age which is not observed; our reported developmental patterns are consistent during this age. Finally, although a recent EEG study reported that functional connectivity differs between quiet sleep and active sleep among newborns (103), this study recorded EEG signals for a much longer duration (40-90 mins) than our rsfMRI scanning (5 mins) to cover active and quiet sleep. In fact, for a typical 1-hour sleep cycle of a newborn, the sleeping duration for one state may last up to 30 minutes, which is much longer than our scanning time, suggesting that it is plausible that rsfMRI data may be within a single sleeping state.

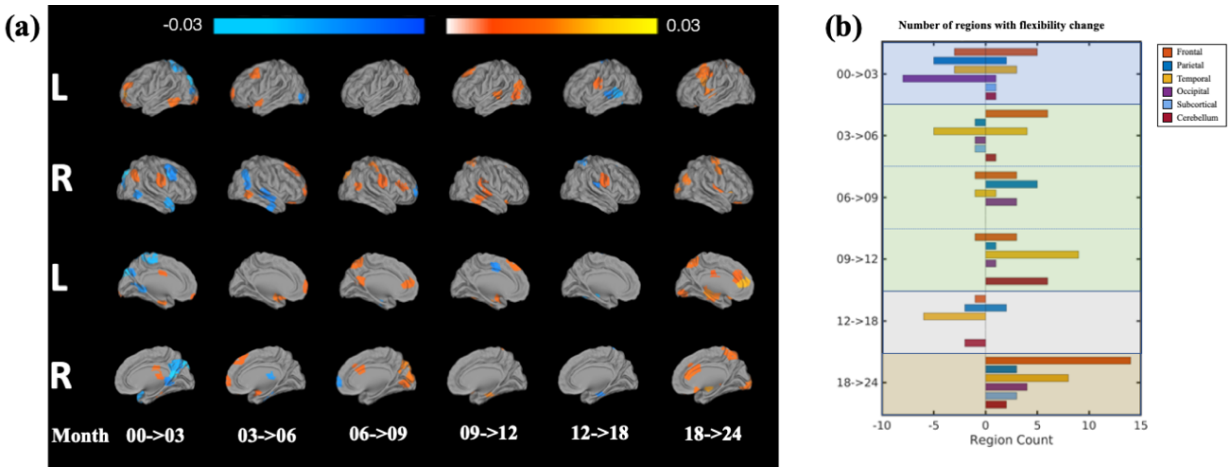

Fig. S1. Neural flexibility changes between every two adjacent age groups (two sample T-test, $p < 0.05$, uncorrected). (a) Brain regions exhibit statistical changes of neural flexibility between two contiguous age groups ($p < 0.05$, uncorrected). (b) Number of brain regions changing neural flexibility between two adjacent age groups summarized by brain lobes. The developmental pattern separates into four age periods (month 00 to 03 (blue); month 03 to 12 (green); month 12 to 18 (gray); and month 18 to 24 (brown)).

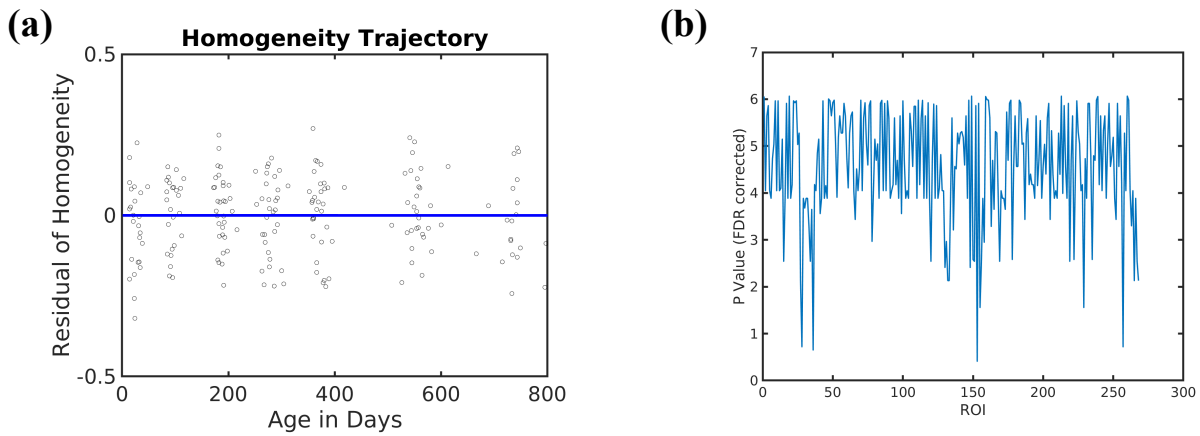

Fig. S2. (a) A representative example of homogeneity trajectory for a given brain region, demonstrating no clear age effects. The blue line is the LME fitted trajectory. (b) The FDR corrected p-values (LME model, F-test) for all the ROIs.

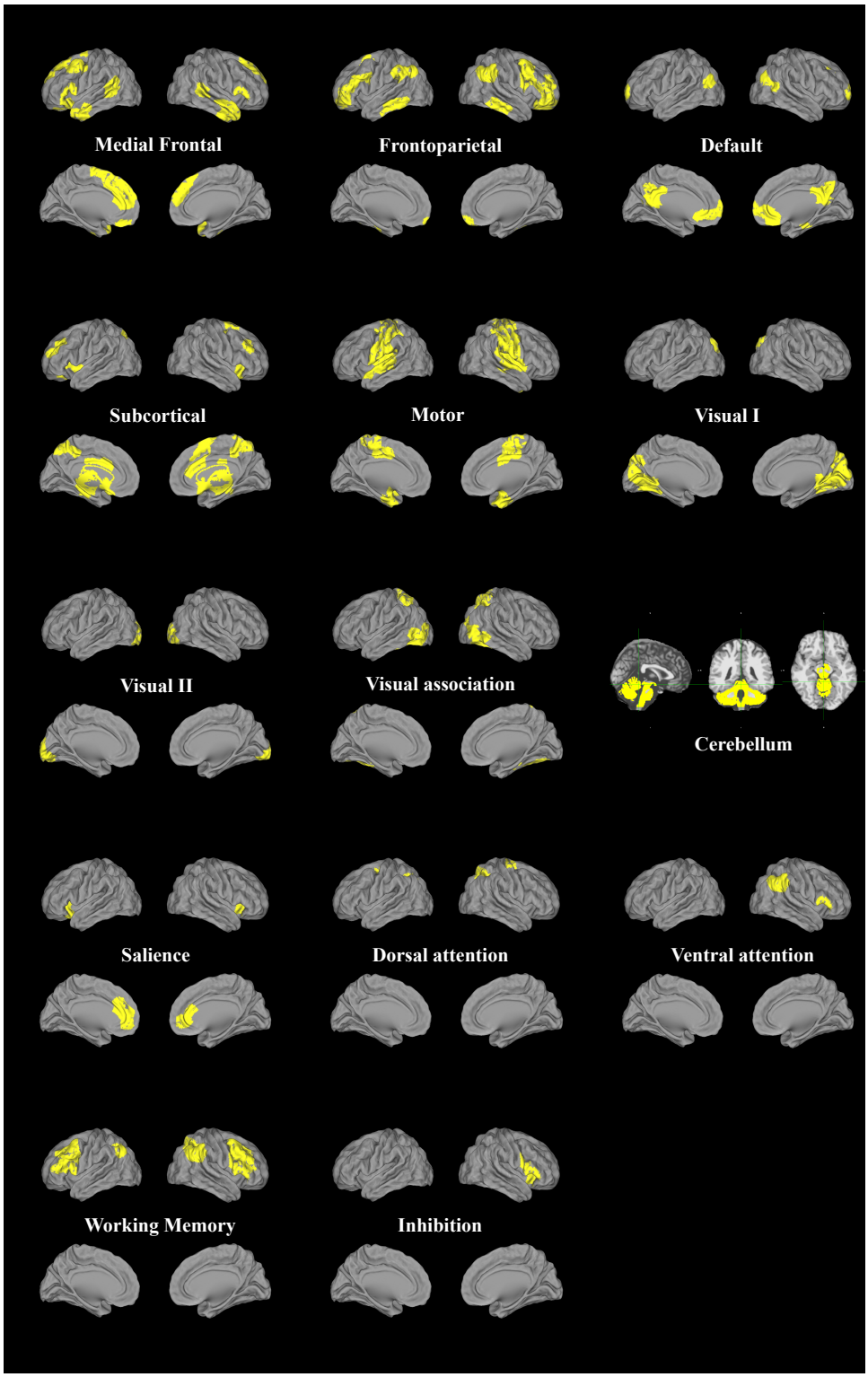

Fig. S3. The anatomical regions of each brain network employed in our study.

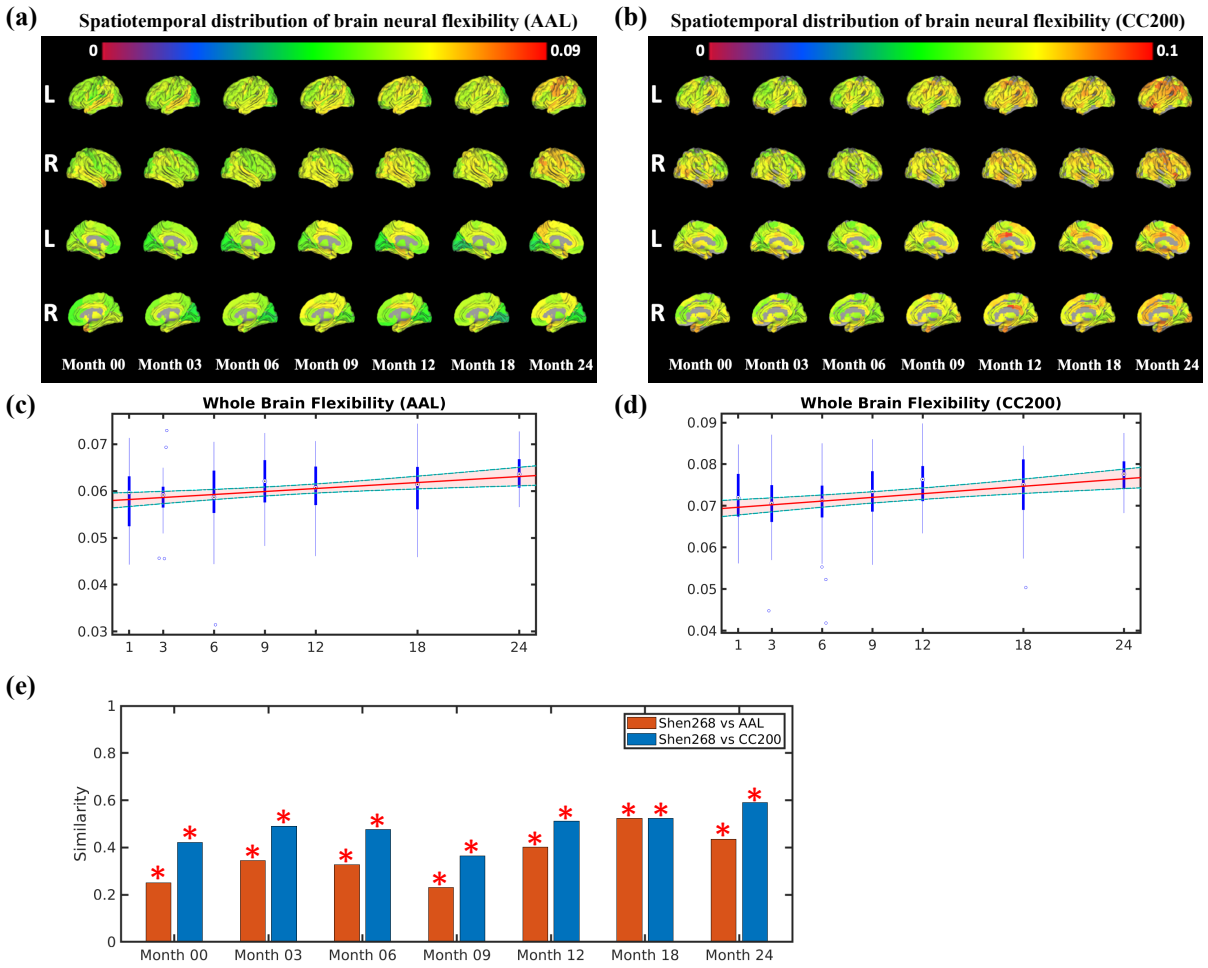

Fig. S4. Spatiotemporal distributions of regional neural flexibility using the AAL atlas (a) and the CC200 atlas (b), respectively. The developmental trajectories of the whole brain neural flexibility using the AAL atlas (c) (LME model, F-test, F(1,201)=11.2, $p = 0.0009$) and the CC200 atlas (d) (LME model, F-test, F(1,201)=18.13, $p = 3.15 \times 10^{-5}$), respectively. (e) Voxel-wise spatial similarity between Shen268 and AAL atlases, as well as between Shen268 and CC200 atlases among different ages (significance level: $*$ $p < 10^{-16}$, FDR corrected).

(a)

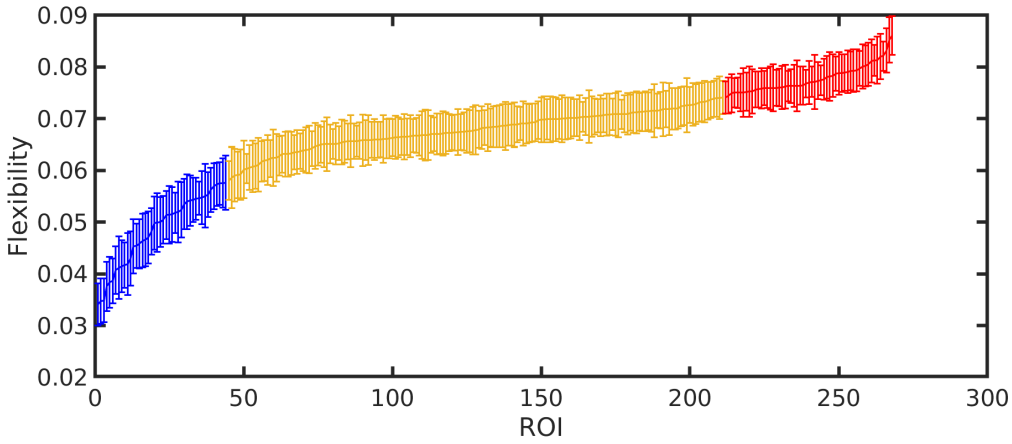

(b)

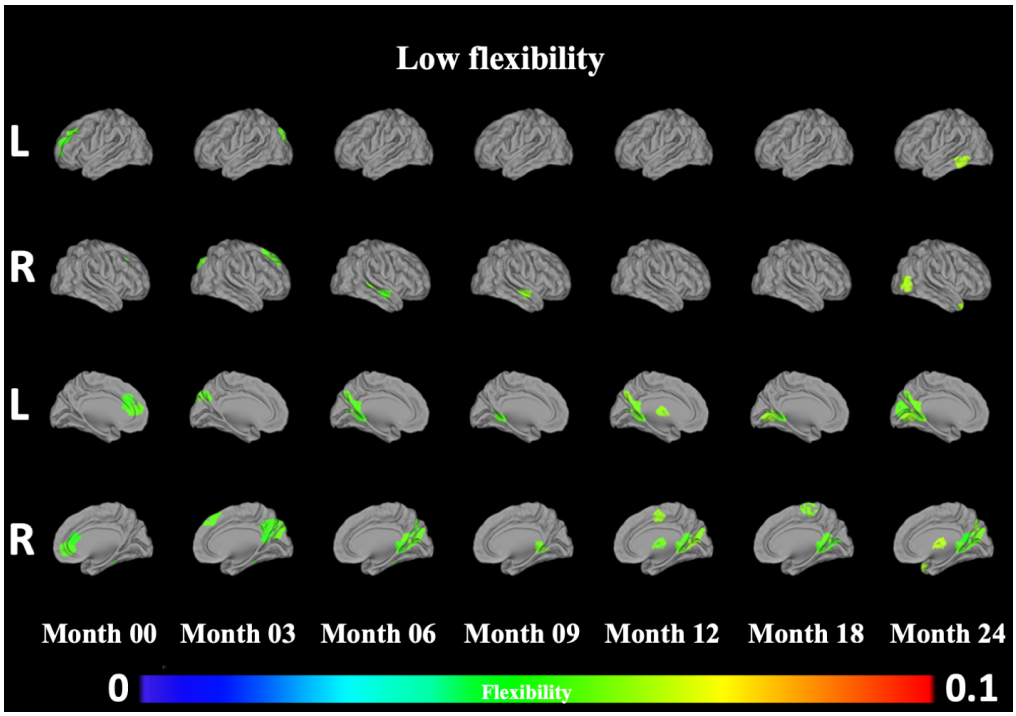

Fig. S5. (a) Ranked regional flexibility, which separates into three groups: red/blue indicate significantly higher/lower neural flexibility when compared to the whole brain neural flexibility, respectively; and orange indicates regions that are not significantly different from that of the whole brain, $p < 0.05$, uncorrected). (b) Spatial distribution of brain regions with significantly lower flexibility than that of the whole brain ($p < 0.05$, uncorrected).

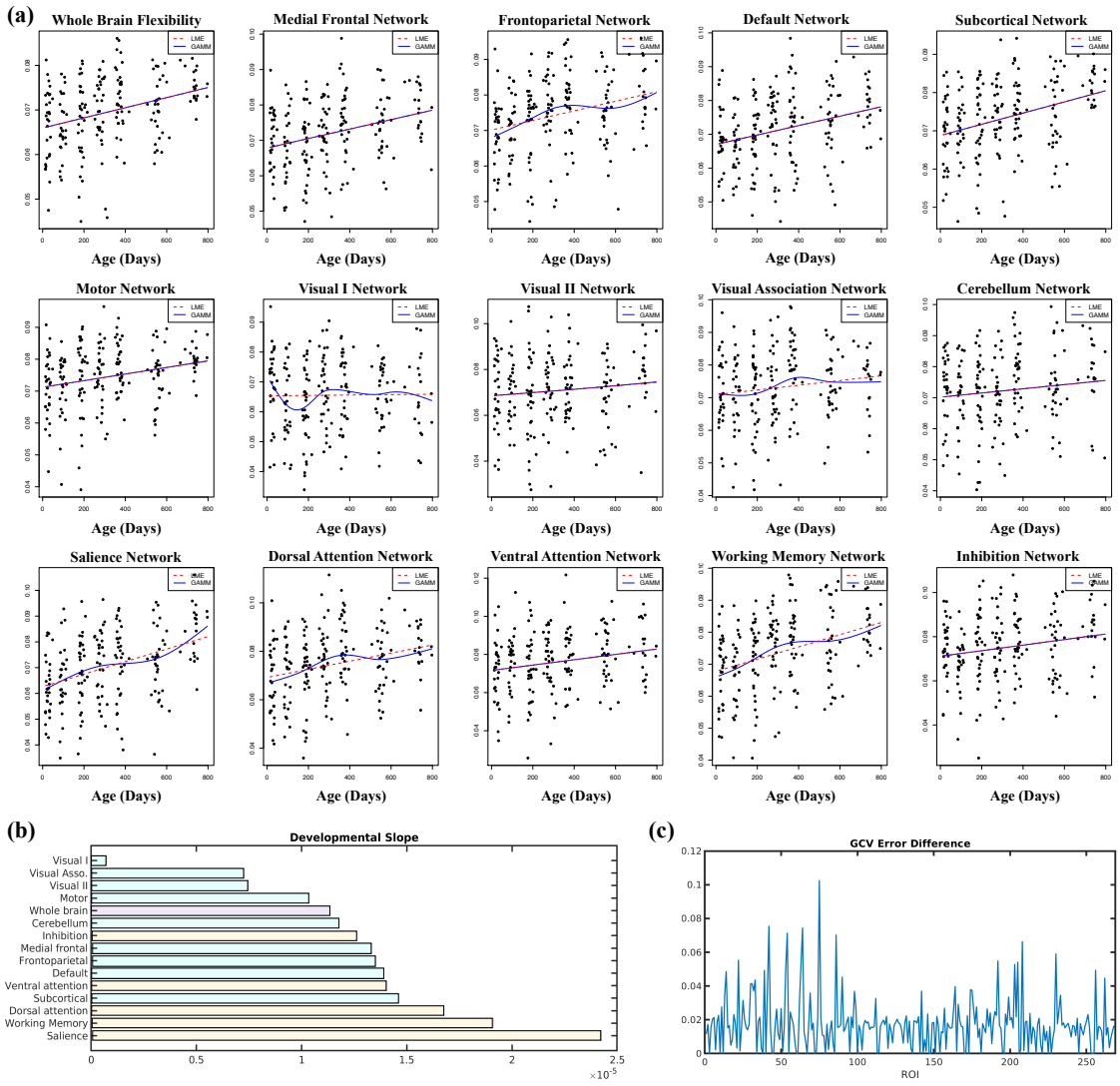

Fig. S6. Developmental model selection between LME and GAMM. (a) Developmental trajectories of neural flexibility using both the LME and GAMM models for the whole brain, nine resting-state functional networks, and five cognitive flexibility related networks. (b) The developmental slopes of the neural flexibility of whole brain and different brain networks (LME model), sorted by the slopes. (C) The GCV error difference of LME and GAMM model across difference ROIs.

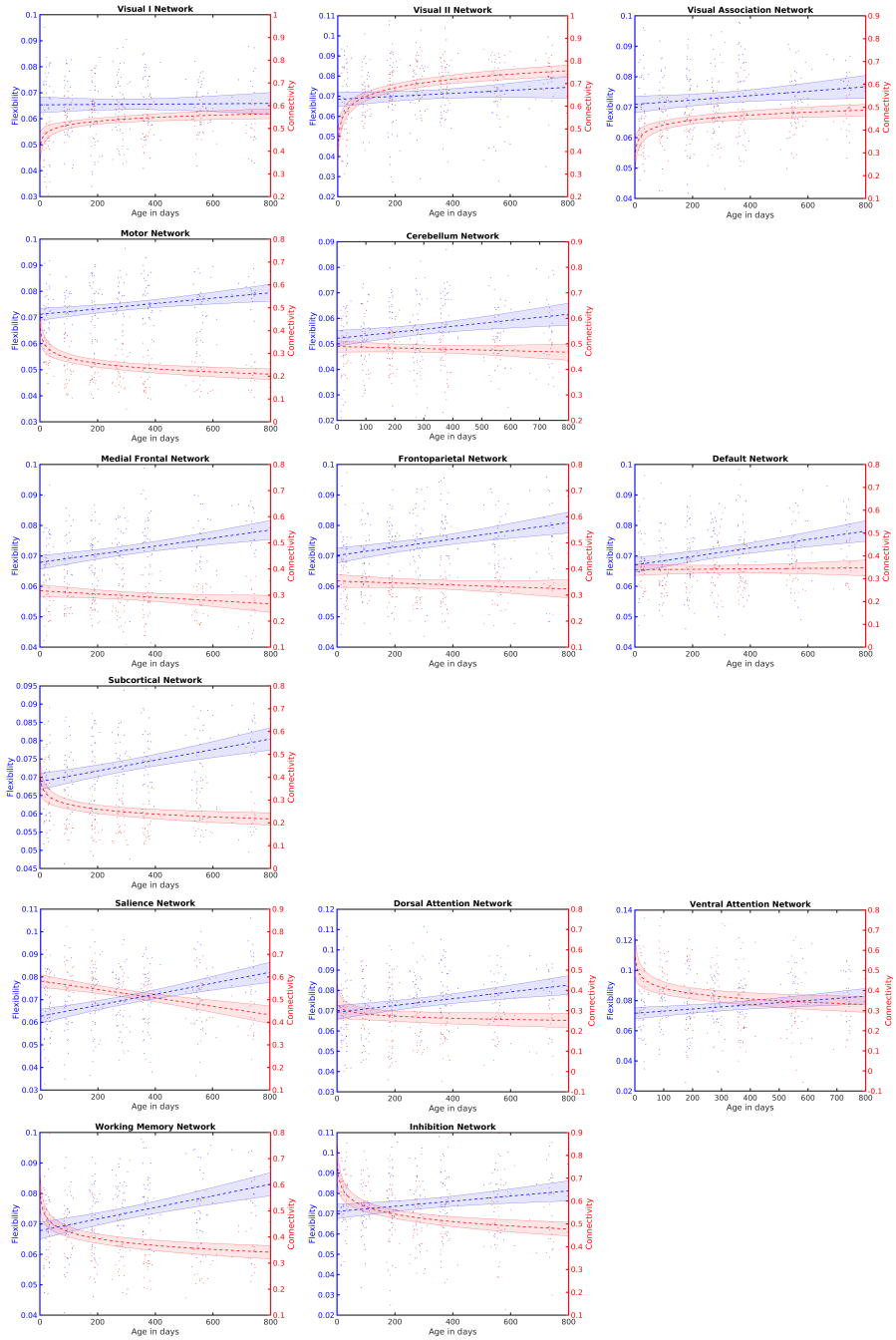

Fig. S7. The developmental trajectories of network flexibility and functional connectivity. Blue lines represent flexibility developmental trajectories ($p_{VisI} = 1$, $p_{VisII} = 0.48$, $p_{VisAssoc.} = 0.13$, $p_{motor} = 0.003$, $p_{cerebellum} = 0.015$, $p_{MFN} = 4.61 \times 10^{-5}$, $p_{FPN} = 0.00015$, $p_{DMN} = 8.66 \times 10^{-5}$, $p_{Subcortical} = 3.44 \times 10^{-6}$, $p_{Salience} = 8.24 \times 10^{-7}$, $p_{DorsalAtten.} = 0.0005$, $p_{VentralAtten.} = 0.013$, $p_{WorkingMemory} = 8.86 \times 10^{-7}$, $p_{Inhibition} = 0.022$, FDR corrected). Red lines represent connectivity developmental trajectories ($p_{VisI} = 0.0013$, $p_{VisII} = 3.2 \times 10^{-12}$, $p_{VisAssoc.} = 8.4 \times 10^{-5}$, $p_{motor} = 2.02 \times 10^{-6}$, $p_{cerebellum} = 1$, $p_{MFN} = 0.17$, $p_{FPN} = 0.81$, $p_{DMN} = 2.41$, $p_{Subcortical} = 0.0002$, $p_{Salience} = 9.6 \times 10^{-6}$, $p_{DorsalAtten.} = 0.4$, $p_{VentralAtten.} = 0.0012$, $p_{WorkingMemory} = 1.09 \times 10^{-6}$, $p_{Inhibition} = 2.78 \times 10^{-6}$, FDR corrected).

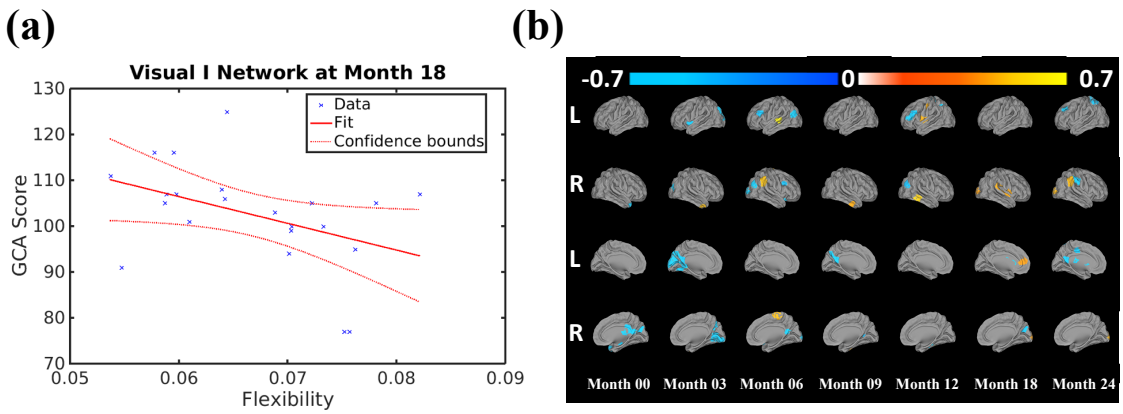

Fig. S8. Prediction of later behavioral performance using neural flexibility. (a) Visual I network at month 18 was correlated with the GCA scores (Pearson's correlation T-test, t(20)=-2.08, $p = 0.019$, uncorrected) at 5/6 years old. (b) Brain region correlate with the GCA scores at 5/6 years old (Pearson's correlation T-test, $p < 0.05$, uncorrected).

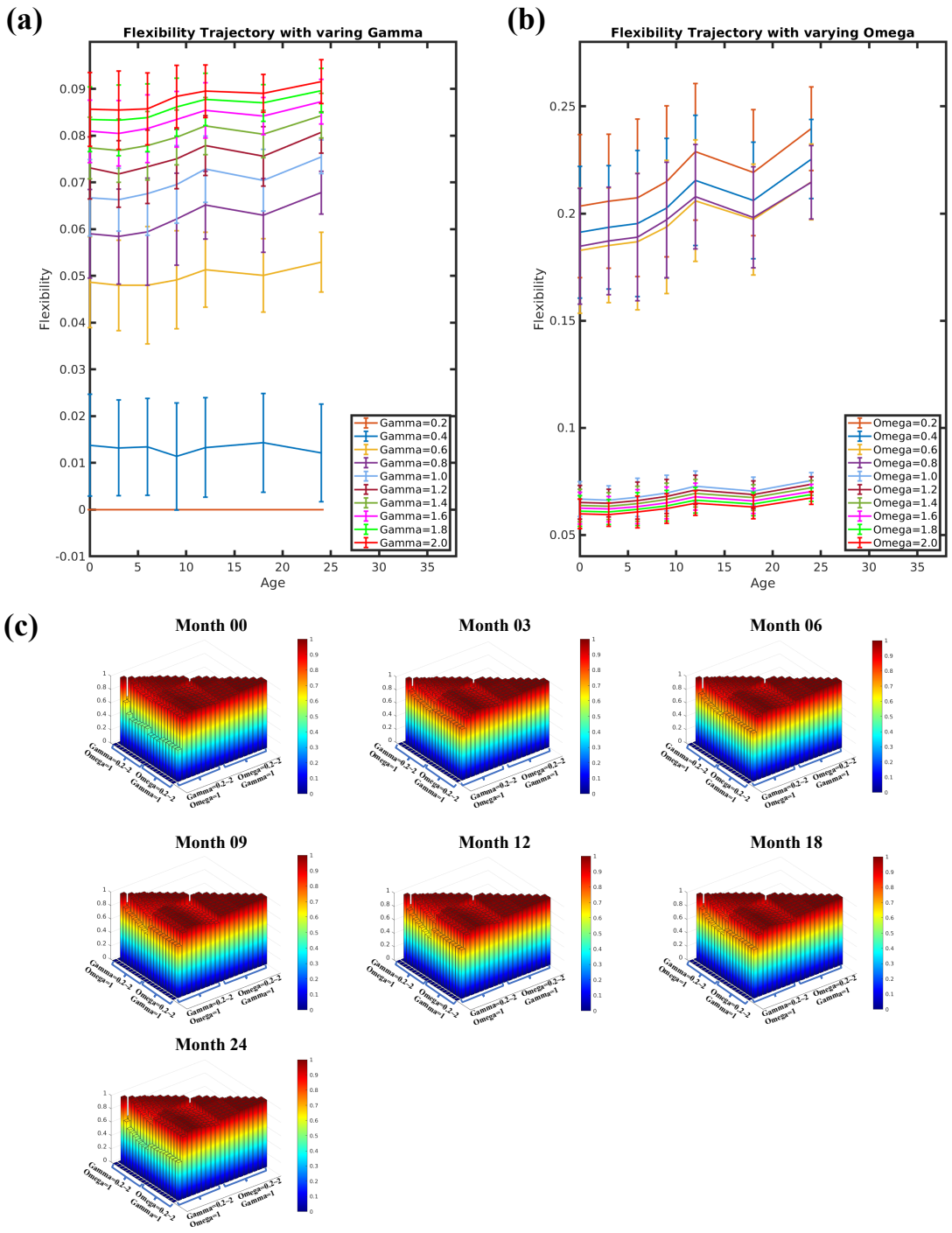

Fig. S9. Effects of the resolution and coupling parameters. (a) Flexibility trajectory with Omega equals to 1 while Gamma varies from 0.2 to 2. (b) Flexibility trajectories with Gamma equals to 1 while varying Omega from 0.2 to 2. (c) Spatial similarity of the regional distribution of brain neural flexibility at different Gammas, Omegas and age groups.

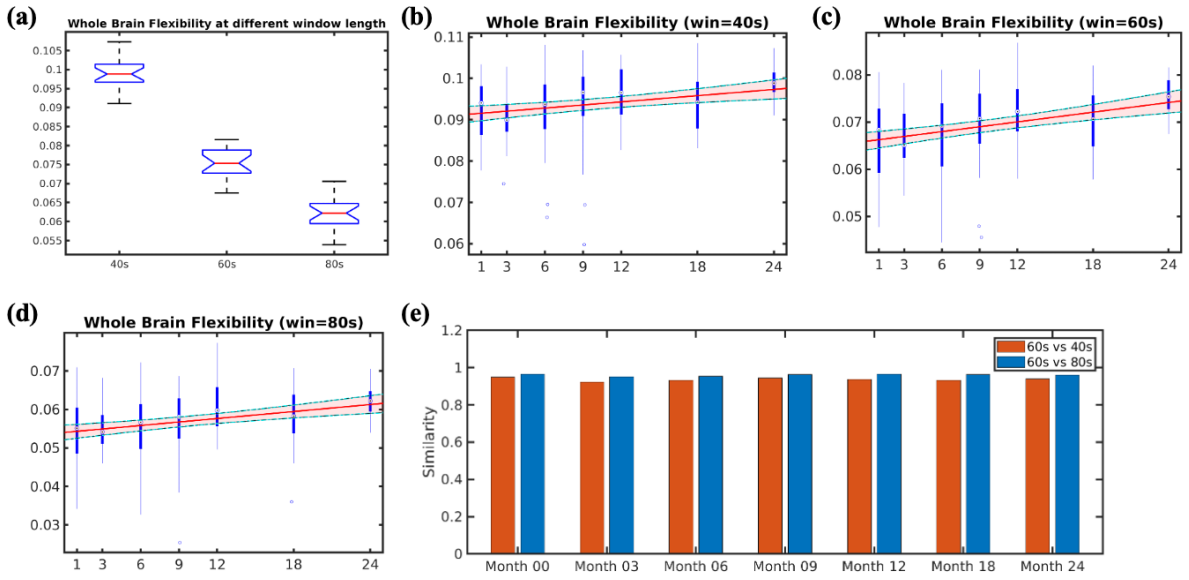

Fig. S10. (a) The effects of window length on neural flexibility. The developmental trajectories of a window length of 40s (LME model, F-test, F(1,201)=12.66, $p = 4.64 \times 10^{-4}$), (c) 60s (LME model, F-test, F(1,201)=25.13, $p = 1.17 \times 10^{-6}$) and (d) 80s (LME model, F-test, F(1,201)=18.71, $p = 2.39 \times 10^{-5}$). (e) Spatial similarity of the distribution of brain neural flexibility (60s vs 40s, 60s vs 80s) among different age groups.

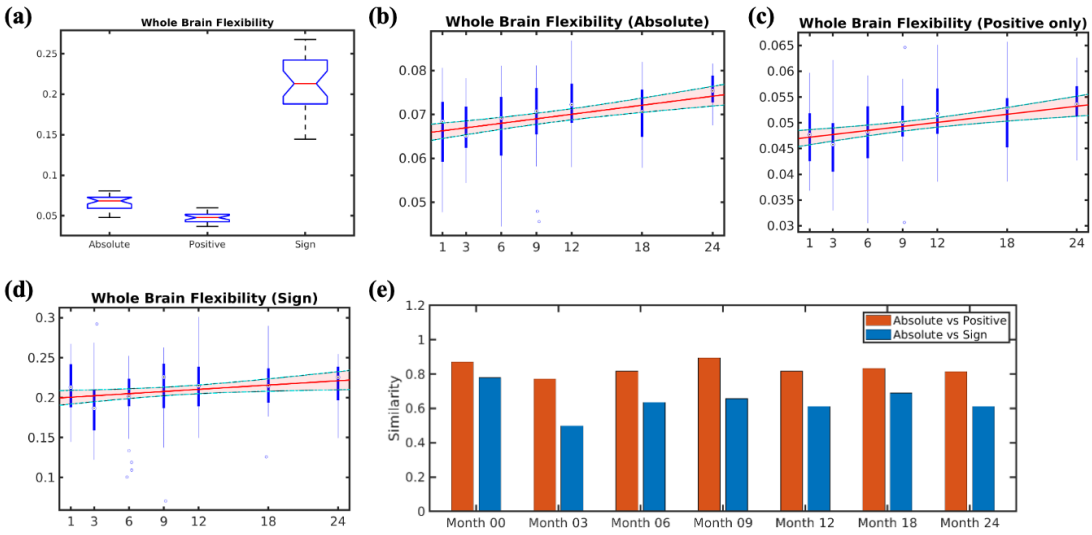

Fig. S11. Comparison of using absolute values, positive-only values and signed values of connectivity. (a) The estimated neural flexibility when absolute values, positive-only values, signed values of connectivity were employed, respectively. (b) The developmental trajectory of using absolute values of connectivity (LME model, F-test, F(1,201)=25.13, $p = 1.17 \times 10^{-6}$). (c) The developmental trajectory of using positive-only connectivity (LME model, F-test, F(1,201)=17.25, $p = 4.83 \times 10^{-5}$). (d) The developmental trajectory of using signed values of connectivity (LME model, F-test, F(1,201)=5.9, $p = 0.016$). (e) Spatial similarity of the distribution of brain neural flexibility (absolute vs positive only, red and absolute vs signed, blue) among different age groups.

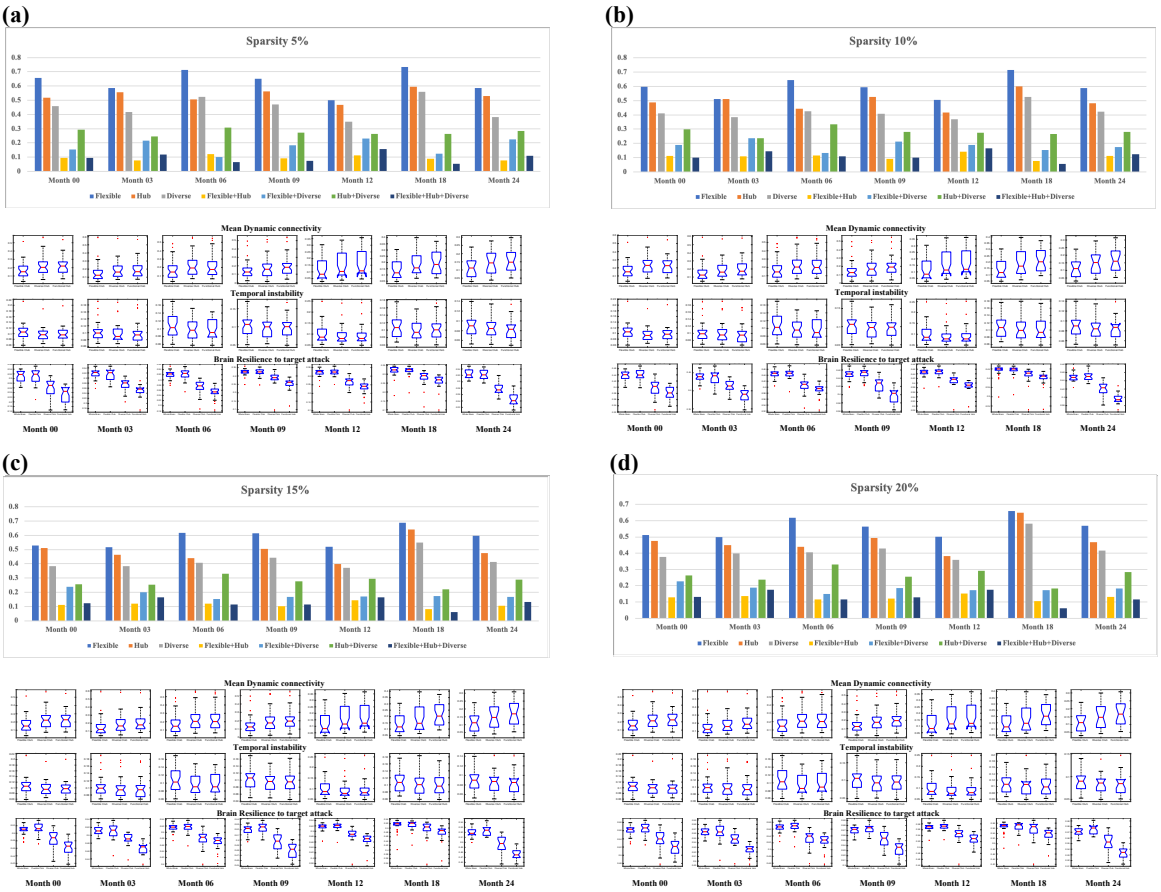

Fig. S12. Comparison of flexible club, functional hub and diverse club at different age group, as well as different sparsity choice: (a) 5%, (b) 10%, (c) 15% and (d) 20%. Comparison includes spatial overlapping ratios across brain flexible club, functional hub and diverse club, statistical comparisons of the mean dynamic connectivity strengths, standard deviations of dynamic connectivity, among the flexible club, functional hub and diverse club, as well as the impacts on global efficiency after removing flexible club, functional hub and diverse club.

Table S1. Summary of regions with significantly higher/lower neural flexibility than that of the whole brain

	Month 00	Month 03	Month 06	Month 09	Month 12	Month 18	Month 24
Higher than whole brain	57	55	54	54	66	43	59
Lower than whole brain	44	45	50	47	46	45	48

Table S2. Comparisons between GAMM and LME

	GAMM			LME			Difference
Parameter	***AIC***	***Rsquare***	***GCV***	***AIC***	***Rsquare***	***GCV***	***GCV***
Whole Brain	-1422.3349	0.22456559	5.31E-05	-1412.958	0.23211518	5.37E-05	1.12%
Medial Frontal Network	-1335.1269	0.18376478	8.13E-05	-1328.2243	0.19385009	8.24E-05	1.34%
Frontoparietal Network	-1301.0789	0.21404696	9.67E-05	-1288.8818	0.18980874	9.97E-05	3.01%
Default Network	-1301.0078	0.18762543	9.64E-05	-1293.7371	0.18919057	9.76E-05	1.23%
Subcortical Network	-1347.453	0.2405714	7.69E-05	-1337.3176	0.24686581	7.79E-05	1.28%
Motor Network	-1315.5924	0.11823484	8.93E-05	-1310.976	0.1231795	9.07E-05	1.54%
Visual I network	-1225.1044	0.18739155	0.00014143	-1207.439	0.12679354	0.00014871	4.90%
Visual II Network	-1109.3427	0.00633059	0.00024546	-1107.3349	0.01080285	0.00024547	0.00%
Visual Association Network	-1258.1619	0.14138781	0.00011935	-1249.9411	0.13436138	0.00012119	1.52%
Cerebellum Network	-1196.1418	0.11174869	0.00016081	-1191.2728	0.11445419	0.00016308	1.39%
Salience Network	-1184.2196	0.16995432	0.00016997	-1179.9917	0.16454121	0.00017469	2.70%
Dorsal Attention Network	-1181.36	0.22799297	0.00017503	-1167.3451	0.19381532	0.00018086	3.22%
Ventral Attention Network	-1134.2109	0.20091478	0.0002203	-1122.45	0.20487582	0.00022281	1.13%
Working Memory Network	-1267.7872	0.2921376	0.00011457	-1252.4132	0.27764675	0.00011734	2.37%
Inhibition Network	-1145.4177	0.14636654	0.00020747	-1137.8915	0.14603929	0.00021031	1.35%

SI Reference

1. H. Lu, S. Jaime, Y. Yang, Origins of the Resting-State Functional MRI Signal: Potential Limitations of the “Neurocentric” Model. *Frontiers in Neuroscience* **13** (2019).
2. A. Z. Snyder, M. E. Raichle, A brief history of the resting state: the Washington University perspective. *NeuroImage* **62**, 902-910 (2012).
3. R. M. Hutchison, J. B. Morton, Tracking the Brain's Functional Coupling Dynamics over Development. *The Journal of neuroscience : the official journal of the Society for Neuroscience* **35**, 6849-6859 (2015).
4. E. A. Allen *et al.*, Tracking whole-brain connectivity dynamics in the resting state. *Cerebral cortex* **24**, 663-676 (2014).
5. E. Damaraju *et al.*, Dynamic functional connectivity analysis reveals transient states of dysconnectivity in schizophrenia. *Neuroimage-Clin* **5**, 298-308 (2014).
6. J. R. Cohen, The behavioral and cognitive relevance of time-varying, dynamic changes in functional connectivity. *NeuroImage* **180**, 515-525 (2018).
7. P. Delamillieure *et al.*, The resting state questionnaire: An introspective questionnaire for evaluation of inner experience during the conscious resting state. *Brain Res Bull* **81**, 565-573 (2010).
8. G. Doucet *et al.*, Patterns of hemodynamic low-frequency oscillations in the brain are modulated by the nature of free thought during rest. *NeuroImage* **59**, 3194-3200 (2012).
9. N. Leonardi, D. Van De Ville, On spurious and real fluctuations of dynamic functional connectivity during rest. *NeuroImage* **104**, 430-436 (2015).
10. A. Zalesky, M. Breakspear, Towards a statistical test for functional connectivity dynamics. *NeuroImage* **114**, 466-470 (2015).
11. R. M. Hutchison *et al.*, Dynamic functional connectivity: promise, issues, and interpretations. *NeuroImage* **80**, 360-378 (2013).
12. R. M. Hutchison, T. Womelsdorf, J. S. Gati, S. Everling, R. S. Menon, Resting-state networks show dynamic functional connectivity in awake humans and anesthetized macaques. *Human brain mapping* **34**, 2154-2177 (2013).
13. W. R. Shirer, S. Ryali, E. Rykhlevskaia, V. Menon, M. D. Greicius, Decoding Subject-Driven Cognitive States with Whole-Brain Connectivity Patterns. *Cerebral cortex* **22**, 158-165 (2011).
14. A. X. Patel *et al.*, A wavelet method for modeling and despiking motion artifacts from resting-state fMRI time series. *NeuroImage* **95**, 287-304 (2014).
15. A. X. Patel, E. T. Bullmore, A wavelet-based estimator of the degrees of freedom in denoised fMRI time series for probabilistic testing of functional connectivity and brain graphs. *NeuroImage* **142**, 14-26 (2016).
16. D. S. Bassett *et al.*, Dynamic reconfiguration of human brain networks during learning. *Proceedings of the National Academy of Sciences of the United States of America* **108**, 7641-7646 (2011).
17. U. Braun *et al.*, Dynamic reconfiguration of frontal brain networks during executive cognition in humans. *Proceedings of the National Academy of Sciences of the United States of America* **112**, 11678-11683 (2015).
18. U. Braun *et al.*, Dynamic brain network reconfiguration as a potential schizophrenia genetic risk mechanism modulated by NMDA receptor function. *Proceedings of the National Academy of Sciences of the United States of America* **113**, 12568-12573 (2016).
19. M. Pedersen, A. Zalesky, A. Omidvarnia, G. D. Jackson, Multilayer network switching rate predicts brain performance. *Proceedings of the National Academy of Sciences of the United States of America* **115**, 13376-13381 (2018).
20. E. S. Finn *et al.*, Functional connectome fingerprinting: identifying individuals using patterns of brain connectivity. *Nature Neuroscience* **18**, 1664-1671 (2015).
21. R. C. Craddock, G. A. James, P. E. Holtzheimer, X. P. P. Hu, H. S. Mayberg, A whole brain fMRI atlas generated via spatially constrained spectral clustering. *Human brain mapping* **33**, 1914-1928 (2012).
22. Jonathan D. Power *et al.*, Functional Network Organization of the Human Brain. *Neuron* **72**, 665-678 (2011).

23. B. T. Yeo *et al.*, The organization of the human cerebral cortex estimated by intrinsic functional connectivity. *Journal of neurophysiology* **106**, 1125-1165 (2011).
24. F. Shi *et al.*, Infant brain atlases from neonates to 1- and 2-year-olds. *PloS one* **6**, e18746 (2011).
25. I. S. Gousias *et al.*, Automatic segmentation of brain MRIs of 2-year-olds into 83 regions of interest. *NeuroImage* **40**, 672-684 (2008).
26. F. Shi, A. P. Salzwedel, W. Lin, J. H. Gilmore, W. Gao, Functional Brain Parcellations of the Infant Brain and the Associated Developmental Trends. *Cerebral cortex* 10.1093/cercor/bhx062, 1-11 (2017).
27. B. Alexander *et al.*, A new neonatal cortical and subcortical brain atlas: the Melbourne Children's Regional Infant Brain (M-CRIB) atlas. *NeuroImage* **147**, 841-851 (2017).
28. M. L. Seghier, F. Lazeyras, P. S. Huppi, Functional MRI of the newborn. *Semin Fetal Neonatal Med* **11**, 479-488 (2006).
29. P. Born *et al.*, Visual Activation in Infants and Young Children Studied by Functional Magnetic Resonance Imaging. *Pediatric Research* **44**, 578-583 (1998).
30. E. Martin *et al.*, Visual Processing in Infants and Children Studied Using Functional MRI. *Pediatric Research* **46**, 135-140 (1999).
31. N. R. Altman, B. Bernal, Brain Activation in Sedated Children: Auditory and Visual Functional MR Imaging. *Radiology* **221**, 56-63 (2001).
32. A. W. Anderson *et al.*, Neonatal auditory activation detected by functional magnetic resonance imaging. *Magnetic Resonance Imaging* **19**, 1-5 (2001).
33. S. G. Erberich *et al.*, Somatosensory lateralization in the newborn brain. *NeuroImage* **29**, 155-161 (2006).
34. P. Born, E. Rostrup, H. Leth, B. Peitersen, H. C. Lou, Change of visually induced cortical activation patterns during development. *Lancet* **347**, 543 (1996).
35. A. P. Born *et al.*, Functional magnetic resonance imaging of the normal and abnormal visual system in early life. *Neuropediatrics* **31**, 24-32 (2000).
36. S. Muramoto *et al.*, Age-Dependent Change in Metabolic Response to Photic Stimulation of the Primary Visual Cortex in Infants: Functional Magnetic Resonance Imaging Study. *Journal of Computer Assisted Tomography* **26**, 894-901 (2002).
37. T. Morita *et al.*, Difference in the metabolic response to photic stimulation of the lateral geniculate nucleus and the primary visual cortex of infants: a fMRI study. *Neuroscience Research* **38**, 63-70 (2000).
38. L. T. L. Sie *et al.*, Functional MRI of visual cortex in sedated 18 month-old infants with or without periventricular leukomalacia. *Developmental Medicine & Child Neurology* **43**, 486-490 (2001).
39. W. Gao *et al.*, Temporal and Spatial Evolution of Brain Network Topology during the First Two Years of Life. *PloS one* **6**, e25278 (2011).
40. P. T. Yap *et al.*, Development trends of white matter connectivity in the first years of life. *PloS one* **6**, e24678 (2011).
41. X. Wen *et al.*, First-year development of modules and hubs in infant brain functional networks. *NeuroImage* **185**, 222-235 (2019).
42. E. M. Gordon *et al.*, Generation and Evaluation of a Cortical Area Parcellation from Resting-State Correlations. *Cerebral cortex* **26**, 288-303 (2016).
43. S. M. Smith *et al.*, Correspondence of the brain's functional architecture during activation and rest. *Proceedings of the National Academy of Sciences of the United States of America* **106**, 13040-13045 (2009).
44. D. R. Dajani, L. Q. Uddin, Demystifying cognitive flexibility: Implications for clinical and developmental neuroscience. *Trends Neurosci* **38**, 571-578 (2015).
45. L. Q. Uddin, Salience processing and insular cortical function and dysfunction. *Nat Rev Neurosci* **16**, 55-61 (2015).
46. M. Corbetta, G. L. Shulman, Control of goal-directed and stimulus-driven attention in the brain. *Nat Rev Neurosci* **3**, 201-215 (2002).
47. M. E. Thomason *et al.*, Development of spatial and verbal working memory capacity in the human brain. *J Cogn Neurosci* **21**, 316-332 (2009).
48. A. R. Aron, R. A. Poldrack, Cortical and subcortical contributions to Stop signal response inhibition: role of the subthalamic nucleus. *The Journal of neuroscience : the official journal of the Society for Neuroscience* **26**, 2424-2433 (2006).

49. P. Fransson *et al.*, Resting-state networks in the infant brain. *Proceedings of the National Academy of Sciences of the United States of America* **104**, 15531-15536 (2007).
50. Y. X. Chang *et al.*, The multi-targets integrated fingerprinting for screening anti-diabetic compounds from a Chinese medicine Jinqi Jiangtang Tablet. *J Ethnopharmacol* **164**, 210-222 (2015).
51. B. R. White, S. M. Liao, S. L. Ferradal, T. E. Inder, J. P. Culver, Bedside optical imaging of occipital resting-state functional connectivity in neonates. *NeuroImage* **59**, 2529-2538 (2012).
52. S. Liao *et al.*, Neonatal hemodynamic response to visual cortex activity: high-density near-infrared spectroscopy study. *Journal of Biomedical Optics* **15**, 026010 (2010).
53. C. F. Dosman, D. Andrews, K. J. Goulden, Evidence-based milestone ages as a framework for developmental surveillance. *Paediatr Child Health* **17**, 561-568 (2012).
54. M. M. Shirley, The first two years: A study of twenty-five babies. (1933).
55. V. Doria *et al.*, Emergence of resting state networks in the preterm human brain. *Proceedings of the National Academy of Sciences of the United States of America* **107**, 20015-20020 (2010).
56. W. Gao *et al.*, Evidence on the emergence of the brain's default network from 2-week-old to 2-year-old healthy pediatric subjects. *Proceedings of the National Academy of Sciences of the United States of America* **106**, 6790-6795 (2009).
57. G. Dehaene-Lambertz, S. Dehaene, L. Hertz-Pannier, Functional neuroimaging of speech perception in infants. *Science* **298**, 2013-2015 (2002).
58. T. Grossmann, R. Oberecker, S. P. Koch, A. D. Friederici, The developmental origins of voice processing in the human brain. *Neuron* **65**, 852-858 (2010).
59. T. Grossmann, Shedding light on infant brain function: the use of near-infrared spectroscopy (NIRS) in the study of face perception. *Acta Paediatrica* **97**, 1156-1158 (2008).
60. Y. Saito *et al.*, Frontal cerebral blood flow change associated with infant-directed speech. *Arch Dis Child Fetal Neonatal Ed* **92**, F113-F116 (2007).
61. J. Carlsson, H. Lagercrantz, L. Olson, G. Printz, M. Bartocci, Activation of the right fronto-temporal cortex during maternal facial recognition in young infants. *Acta Paediatrica* **97**, 1221-1225 (2008).
62. T. Grossmann, M. H. Johnson, Selective prefrontal cortex responses to joint attention in early infancy. *Biol Lett* **6**, 540-543 (2010).
63. N. Tzourio-Mazoyer *et al.*, Automated anatomical labeling of activations in SPM using a macroscopic anatomical parcellation of the MNI MRI single-subject brain. *NeuroImage* **15**, 273-289 (2002).
64. J. M. Ye, On measuring and correcting the effects of data mining and model selection. *Journal of the American Statistical Association* **93**, 120-131 (1998).
65. X. H. Lin, D. W. Zhang, Inference in generalized additive mixed models by using smoothing splines. *J Roy Stat Soc B* **61**, 381-400 (1999).
66. M. Sóskuthy, Generalised additive mixed models for dynamic analysis in linguistics: a practical introduction. *eprint arXiv:1703.05339*, arXiv:1703.05339 (2017).
67. W. Gao, S. Alcauter, J. K. Smith, J. H. Gilmore, W. Lin, Development of human brain cortical network architecture during infancy. *Brain structure & function* **220**, 1173-1186 (2015).
68. R. W. Emerson, W. Gao, W. Lin, Longitudinal Study of the Emerging Functional Connectivity Asymmetry of Primary Language Regions during Infancy. *The Journal of neuroscience : the official journal of the Society for Neuroscience* **36**, 10883-10892 (2016).
69. S. Shultz, A. Vouloumanos, R. H. Bennett, K. Pelphrey, Neural specialization for speech in the first months of life. *Dev Sci* **17**, 766-774 (2014).
70. S. Marcovitch, M. W. Clearfield, M. Swingler, S. D. Calkins, M. A. Bell, Attentional Predictors of 5-month-olds' Performance on a Looking A-not-B Task. *Infant Child Dev* **25**, 233-246 (2016).
71. L. M. Oakes, H. A. Baumgartner, S. Kanjlia, S. J. Luck, An eye tracking investigation of color-location binding in infants' visual short-term memory. *Infancy* **22**, 584-607 (2017).
72. M. K. Kwon, S. J. Luck, L. M. Oakes, Visual short-term memory for complex objects in 6- and 8-month-old infants. *Child Dev* **85**, 564-577 (2014).
73. M. E. Lamb, Parent-infant interaction in 8-month-olds. *Child Psychiatry Hum Dev* **7**, 56-63 (1976).
74. K. Cuevas, M. A. Bell, Infant attention and early childhood executive function. *Child Dev* **85**, 397-404 (2014).

75. B. J. Casey *et al.*, The Adolescent Brain Cognitive Development (ABCD) study: Imaging acquisition across 21 sites. *Developmental cognitive neuroscience* **32**, 43-54 (2018).
76. D. C. Van Essen *et al.*, The WU-Minn Human Connectome Project: an overview. *NeuroImage* **80**, 62-79 (2013).
77. M. A. Bertolero, B. T. T. Yeo, M. D'Esposito, The diverse club. *Nat Commun* **8**, 1277 (2017).
78. V. D. Blondel, J.-L. Guillaume, R. Lambiotte, E. Lefebvre, Fast unfolding of communities in large networks. *Journal of Statistical Mechanics: Theory and Experiment* **2008**, P10008 (2008).
79. W. H. Weir, S. Emmons, R. Gibson, D. Taylor, P. J. Mucha, Post-Processing Partitions to Identify Domains of Modularity Optimization. *Algorithms* **10**, 93 (2017).
80. P. J. Mucha, T. Richardson, K. Macon, M. A. Porter, J. P. Onnela, Community structure in time-dependent, multiscale, and multiplex networks. *Science* **328**, 876-878 (2010).
81. D. S. Bassett *et al.*, Task-based core-periphery organization of human brain dynamics. *PLoS Comput Biol* **9**, e1003171 (2013).
82. H. Zhang *et al.* (2018) Multi-layer Large-Scale Functional Connectome Reveals Infant Brain Developmental Patterns. in *Medical Image Computing and Computer Assisted Intervention – MICCAI 2018*, eds A. F. Frangi, J. A. Schnabel, C. Davatzikos, C. Alberola-López, G. Fichtinger (Springer International Publishing, Cham), pp 136-144.
83. J. R. Sato, C. M. Sato, M. K. D. Silva, C. E. Biazoli Commute Time as a Method to Explore Brain Functional Connectomes. *Brain connectivity* **9**, 155-161 (2019).
84. J. Meier *et al.*, A Mapping Between Structural and Functional Brain Networks. *Brain connectivity* **6**, 298-311 (2016).
85. R. L. van den Brink *et al.*, Catecholaminergic Neuromodulation Shapes Intrinsic MRI Functional Connectivity in the Human Brain. *The Journal of Neuroscience* **36**, 7865-7876 (2016).
86. S. Achard, E. Bullmore, Efficiency and cost of economical brain functional networks. *PLoS Comput Biol* **3**, e17 (2007).
87. E. Eldar, J. D. Cohen, Y. Niv, The effects of neural gain on attention and learning. *Nat Neurosci* **16**, 1146-1153 (2013).
88. N. Li *et al.*, Resting-state functional connectivity predicts impulsivity in economic decision-making. *The Journal of neuroscience : the official journal of the Society for Neuroscience* **33**, 4886-4895 (2013).
89. J. D. Rudie *et al.*, Altered functional and structural brain network organization in autism. *NeuroImage: Clinical* **2**, 79-94 (2013).
90. K. A. Garrison *et al.*, Effortless awareness: using real time neurofeedback to investigate correlates of posterior cingulate cortex activity in meditators' self-report. *Frontiers in human neuroscience* **7**, 440 (2013).
91. M. N. Hallquist, F. G. Hillary, Graph theory approaches to functional network organization in brain disorders: A critique for a brave new small-world. *Netw Neurosci* **3**, 1-26 (2019).
92. K. Murphy, M. D. Fox, Towards a consensus regarding global signal regression for resting state functional connectivity MRI. *NeuroImage* **154**, 169-173 (2017).
93. M. Rubinov, O. Sporns, Weight-conserving characterization of complex functional brain networks. *NeuroImage* **56**, 2068-2079 (2011).
94. J. Dobbing, J. Sands, Quantitative growth and development of human brain. *Arch Dis Child* **48**, 757-767 (1973).
95. L. Wang *et al.*, Segmentation of neonatal brain MR images using patch-driven level sets. *NeuroImage* **84**, 141-158 (2014).
96. W. LEE *et al.*, Visual functional magnetic resonance imaging of preterm infants. *Developmental Medicine & Child Neurology* **54**, 724-729 (2012).
97. M. J. Rivkin *et al.*, Prolonged T values in newborn versus adult brain: Implications for fMRI studies of newborns. *Magnetic Resonance in Medicine* **51**, 1287-1291 (2004).
98. S. Goksan *et al.*, Optimal echo time for functional MRI of the infant brain identified in response to noxious stimulation. *Magnetic resonance in medicine* **78**, 625-631 (2017).
99. S. M. Smith *et al.*, Resting-state fMRI in the Human Connectome Project. *NeuroImage* **80**, 144-168 (2013).
100. S. G. Horovitz *et al.*, Low frequency BOLD fluctuations during resting wakefulness and light sleep: a simultaneous EEG-fMRI study. *Human brain mapping* **29**, 671-682 (2008).

101. S. G. Horovitz *et al.*, Decoupling of the brain's default mode network during deep sleep. *Proceedings of the National Academy of Sciences of the United States of America* **106**, 11376-11381 (2009).
102. V. L. Schechtman, R. K. Harper, R. M. Harper, Distribution of slow-wave EEG activity across the night in developing infants. *Sleep* **17**, 316-322 (1994).
103. A. Tokariev *et al.*, Large-scale brain modes reorganize between infant sleep states and carry prognostic information for preterms. *Nature Communications* **10**, 2619 (2019).